

*Research paper***Investigation of background noise in the GNSS position time series using spectral analysis – A case study of Nepal Himalaya****Jagat Dwipendra Ray¹, M. Sithartha Muthu Vijayan²,
Walyeldeen Godah^{3*}, Ashok Kumar⁴**^{1,3}Institute of Geodesy and Cartography, 27 Modzelewskiego St., 02-679, Warsaw, Poland¹e-mail: jagat.ray@igik.edu.pl; ORCID: <https://orcid.org/0000-0002-3447-2001>³e-mail: walyeldeen.godah@igik.edu.pl; ORCID: <https://orcid.org/0000-0002-5616-0770>²CSIR -Fourth Paradigm Institute, NAL Belur campus, Wind Tunnel Road,
560 037, Bangalore, Karnataka, India²e-mail: vijayan@csir4pi.in; ORCID: <https://orcid.org/0000-0002-4270-8766>⁴Department of Physics, Tezpur University, 784028, Napaam, Assam, India⁴e-mail: ask@tezu.ernet.in; ORCID: <https://orcid.org/0000-0002-5070-9902>

*Corresponding author: Walyeldeen Godah

Received: 07 October 2019 / Accepted: 18 October 2019

Abstract: Position time series from permanent Global Navigation Satellite System (GNSS) stations are commonly used for estimating secular velocities of discrete points on the Earth's surface. An understanding of background noise in the GNSS position time series is essential to obtain realistic estimates of velocity uncertainties. The current study focuses on the investigation of background noise in position time series obtained from thirteen permanent GNSS stations located in Nepal Himalaya using the spectral analysis method. The power spectrum of the GNSS position time series has been estimated using the Lomb–Scargle method. The iterative nonlinear Levenberg–Marquardt (LM) algorithm has been applied to estimate the spectral index of the power spectrum. The power spectrum can be described by white noise in the high frequency zone and power law noise in the lower frequency zone. The mean and the standard deviation of the estimated spectral indices are -1.46 ± 0.14 , -1.39 ± 0.16 and -1.53 ± 0.07 for north, east and vertical components, respectively. On average, the power law noise extends up to a period of ca. 21 days. For a shorter period, i.e. less than ca. 21 days, the spectra are white. The spectral index corresponding to random walk noise (ca. -2) is obtained for a site located above the base of a seismogenic zone which can be due to the combined effect of tectonic and nontectonic factors rather than a spurious monumental motion. Overall, the usefulness of investigating the background noise in the GNSS position time series is discussed.

Keywords: GNSS, background noise, position time series, spectral analysis© 2019 by the Author(s). Submitted for possible open access publication under the terms and conditions of the Creative Commons Attribution (CC BY-NC) license (<http://creativecommons.org/licenses/by/4.0/>).

1. Introduction

The Global Navigational Satellite System (GNSS) position time series is considered as important geodetic measurements for studying various geophysical phenomena, including plate tectonics and crustal deformation. With the temporal resolution of one day (in most cases), the GNSS position time series carry various types of signals propelled by both tectonic and non-tectonic signals. These signals can be classified into (i) secular, (ii) transients and (iii) seasonal. The secular signal in the geodetic GNSS position time series is the long term plate motion. Transients are class of deformation signal, which can be explained as non-secular, non-periodic accumulation of strain in the crust. Release of the strain energy through earthquake and volcanic eruption generally resulted in transient signal. The seasonal signal is caused by mass transport and mass distribution within the Earth system. The high precision and dense sample warrant the geodetic GNSS position time series are an important resource for monitoring and modelling spatial and temporal variations of station positions due to geodynamic processes, e.g. seismic, volcanic and hydrologic cycles.

Uncertainties of the estimated crustal motion using GNSS measurements depend on the type of noise present in the GNSS position time series. The noise in geodetic time series has been modelled in the frequency domain as a power law process with power spectral density (PSD) of the form f^k where f is the frequency and k is the spectral index (Mandelbrot and Van Ness, 1968; Mandelbrot, 1983). The spectral index k typically falls in the range from -3 to 1 (Agnew, 1992). Random processes within this range are grouped into time correlated and time uncorrelated processes. The processes with spectral index within ± 1 and including special case of white noise ($k = 0$) are called as fractal white noise or fractal Gaussian noise (Amiri-Simkooei et al., 2007). The processes with spectral index $-3 < k < -1$ are called power law noise including special case of random walk noise ($k = -2$) and flicker noise ($k = -1$) (Amiri-Simkooei et al., 2007). The random walk means that the expected value of the position of the GNSS station relative to its earlier position increases as a function of a square root of time (Beavan, 2005). The cause of flicker noise is less clear but long term orbit mismodelling, multipath and time variable satellite geometry have been suggested as possible contributors (Ray et al., 2008; King and Watson 2009; Jiang et al., 2014; Dmitrieva et al., 2015; Bogusz et al., 2018). However, no such error sources have been found to explain the observed level of flicker noise in the GNSS position time series and there is a possibility that flicker noise is caused by surface deformation induced by the seasonal mass loading (Rebischung et al., 2017). Time correlated noise can be estimated from power spectrum of the GNSS position time series (Langbein and Johnson, 1997; Zhang et al., 1997; Santamaría-Gómez et al., 2011). The uncorrelated noise, i.e. white noise, affects the velocity uncertainties which can be reduced through repeated measurements. In order to obtain a reliable estimate of GNSS velocity uncertainty, correlated noise in GNSS position time series should be considered carefully (Johnson and Agnew, 1995; Williams, 2003; Langbein, 2012). The velocity uncertainties were underestimated by a factor of 5–11 if only white noise is assumed to be the background noise in the GNSS position time series (Mao et al., 1999). Santamaría-Gómez et al. (2011) observed from a global GNSS position time se-

ries analysis that mean velocity uncertainty estimates are 4–5 times larger when data are assumed to be time correlated. Wang et al. (2012) revealed that when a pure white noise model is assumed velocity uncertainties were underestimated by a factor of 8–16. Later, Klos et al. (2015) indicated that velocity uncertainties were underestimated if a white noise model is assumed to be the background noise in the GNSS position time series. Therefore, knowledge of background noise in the GNSS position time series is crucial in obtaining realistic velocity uncertainties.

The main objective of this contribution is to investigate the background noise in the GNSS position time series of continuously operated GNSS stations located in Nepal Himalaya that has been established to study the ongoing tectonic deformation at the collision zone of Indian and Eurasian plates. Tectonically active Nepal Himalayan region holds major inland glaciers and undergoes significant deformation due to this hydrological mass loading. The amalgamation of tectonic and non-tectonic signals in the observed GNSS position time series warrants this investigation to characterize the background noise. Accurate quantification of crustal deformation studies of this tectonically active region requires utmost care about the time correlated noise present in the data. Previous study in the Nepal Himalaya like Betinelli et al. (2006) increased the velocity uncertainties by a factor of 3 to accommodate the effects of time correlated noise. Ader et al. (2012) based upon spectral analysis built the data covariance matrix and determined the noise amplitudes by using the Maximum Likelihood Estimation (MLE) algorithm. Later, Ray et al. (2019) used the MLE algorithm to analyze the GNSS time series of Nepal Himalaya for obtaining a possible background noise model. In this study, an investigation has been conducted to analyze the GNSS time series of Nepal Himalaya using the spectral analysis method to obtain the information about the background noise model of the time series.

2. GNSS data processing

Continuous GNSS data from 13 permanent (Table 1, Figure 1) stations located in Nepal Himalaya were analyzed for the period of 2004–2013 using the GAMIT/GLOBK software (Herring et al., 2010).

Daily GNSS data of the aforementioned thirteen continuous GNSS stations were obtained from California Institute of Technology (Caltech) tectonics observatory Nepal network (Avouac et al., 2013). Then these data were checked for quality using the TEQC (Translation, Editing, and Quality Check) software developed by the University NAVSTAR Consortium (UNAVCO). Observation files having less than 12 hours of epoch, high multipath and cycle slips were eliminated from the analysis. GNSS observations of all stations have been kept at an elevation cut off angle of 15° and were sampled at an interval of 30 second. Daily GNSS data from the IGS (International GNSS Service) stations, broadcast ephemeris files and *a priori* orbit files were obtained from the SOPAC (Scripps Orbit and Permanent Array Centre) and the CDDIS (Crustal Dynamics Data Information System). Delays induced by the first order ionospheric refraction were eliminated using linear combination of L1 and L2 signals.

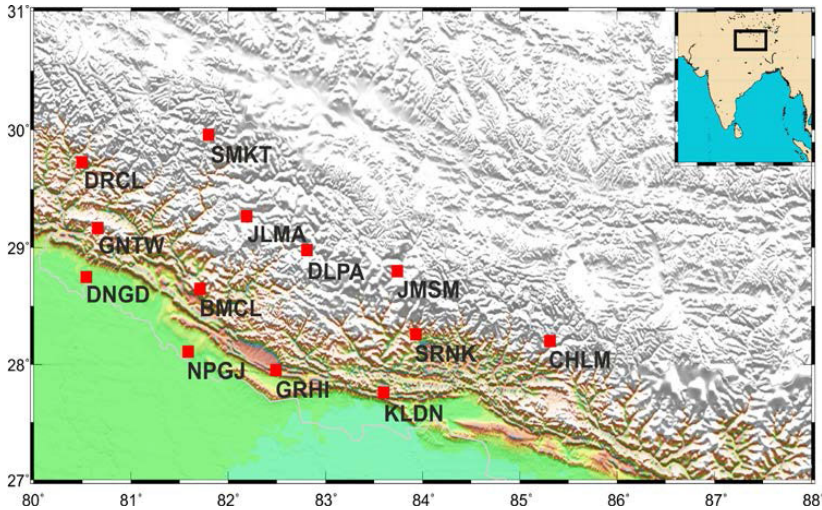


Fig. 1. Study area and the location of permanent GNSS stations used

Table 1. GNSS stations used in the analysis

Site ID	Site Name	Lat [deg]	Long [deg]	Height [m]	Observation Period		
					from	to	no. of obs. days
BMCL	Bhimchula	28.66	81.71	2292.68	2007.20	2013.44	2045
CHLM	Chilime	28.21	85.31	3248.23	2004.24	2013.33	2832
DLPA	Dolpa	28.98	82.82	2569.48	2007.35	2013.24	2123
DNGD	Dhangadi	28.75	80.58	189.12	2008.34	2013.66	1612
DRCL	Darchul	29.73	80.5	2027.33	2008.19	2013.66	1229
GNTW	Ghanteswor	29.18	80.63	2462.64	2008.32	2012.49	891
GRHI	Ghorahi	27.95	82.49	785.33	2007.34	2013.66	2243
JMLA	Jumla	29.28	82.19	2442.11	2007.37	2013.66	2105
JMSM	Jomsom	28.81	83.74	3474.07	2004.33	2012.39	2462
KLDN	Koldana	27.77	83.60	1832.18	2004.28	2012.93	2653
NPGJ	Nepalganj	28.12	81.60	147.83	2007.37	2013.48	2145
SMKT	Simikot	29.97	81.81	3217.12	2008.37	2013.66	1617
SRNK	Sarangkot	28.26	83.94	1701.76	2005.28	2012.42	1397

Daily loose solutions from the GAMIT software were combined with the global files¹ generated by the Massachusetts Institute of Technology (MIT) for definition of

¹<ftp://lox.ucsd.edu/pub/hfiles>

reference frame using the GLORG. No *a priori* noise model was incorporated in the frame defining stage, as the objective of this study is to analysis the noise content in the time series.

The higher order ionospheric delays were applied in the GAMIT software as described in Fritsche et al. (2005). The International Geomagnetic Reference Frame 11 (IGRF11; Finlay et al., 2010) was used to model the magnetic field. The IGRF 11 represents the Earth's main (core) field without external sources and its secular variation through a set of spherical harmonic coefficients. The computation of ionospheric electron content along the signal path (STEC) was achieved by obtaining vertical total electron (VTEC) from daily IONEX (Ionosphere Exchange) files from the Center for Orbit Determination in Europe (CODE)². IONEX files are global ionospheric maps of VTEC in the IONEX format (Schaer et al., 1998) that were generated using a single layer assumption and a mapping function to map STEC to VTEC. To correct the higher order ionospheric delays in GNSS data, “*Ion model = GMAP*” and “*Mag field = IGRF11*” are set in the Session Control Table (sestbl.) of the GAMIT software (Herring et al., 2010).

Tropospheric delay is composed of two parts: (i) dry or hydrostatic delay and (ii) wet delay. The dry component is due to the mixture of all constituents of the troposphere and the mean mass of such a constituent is believed to be equal to the mean mass of all dry components (excluding water vapour). In hydrostatic equilibrium, the zenith delay due to the dry component is modelled using the surface pressure. The second component which is due to the water vapour present along the path of the signal which is tough to quantify through measurements and is predicted by models (Herring et al., 2010). This hindrance is caused by the unmixed condition of atmospheric water vapour which signifies that water vapour can present in “blobs” throughout the troposphere (Herring et al., 2010), making wet delay models inaccurate. Thus, the integrated water vapour along the signal path is parametrically estimated in GNSS processing, which includes the ability to model and estimate zenith delay and its gradient using a piecewise-linear function over the span of the observation. In the GAMIT software, the tropospheric delay is implemented in the following manner

$$TD = ZHD \cdot m_h(\theta) + ZWD \cdot m_w(\theta) \quad (1)$$

where TD is the total delay, ZHD is the zenith hydrostatic delay, m_h is the mapping function corresponding to hydrostatic delay, ZWD is the zenith wet delay, m_w is the mapping function for wet delay and θ is the elevation angle.

Saastamoinen (1972) model was used to compute *a priori* dry zenith delay. The *a priori* model for wet delay is not as critical as wet delay is extracted from GNSS observations, however, it is essential to have a correct mapping function for hydrostatic and wet delay. In this study, the Vienna Mapping Function 1 (VMF1; Kouba, 2008) was used. Incorporation of VMF1 in the GAMIT software requires VMF1 grid files³ which can be invoked by setting *map.grid = Y*, $m_h = \text{VMF1}$ and $m_w = \text{VMF1}$ in the Session Control Table (sestbl.). *A priori* values of pressure and temperature were obtained from the Global Pressure and Temperature (GPT) model (Böhm et al., 2007).

²<ftp://ftp.unibe.ch/aiub/CODE>

³<http://everest.mit.edu>

On the basis of the abovementioned processing strategy, the GNSS position time series of continuous GNSS stations (specified in Table 1) were estimated in the ITRF2008 (International Terrestrial Reference Frame 2008; Altamimi et al., 2011). The time series were detrended, centred and all outliers were removed. Figures 2–4 depict north, east and vertical components of detrended time series of GNSS station positions. The time series (Figures 2–4) are a combination of all kinds of noises, which include the observed seasonal variations. The seasonal variation is more pronounced in the vertical component (Figure 4) than other components and probably caused by the hydrological mass loading.

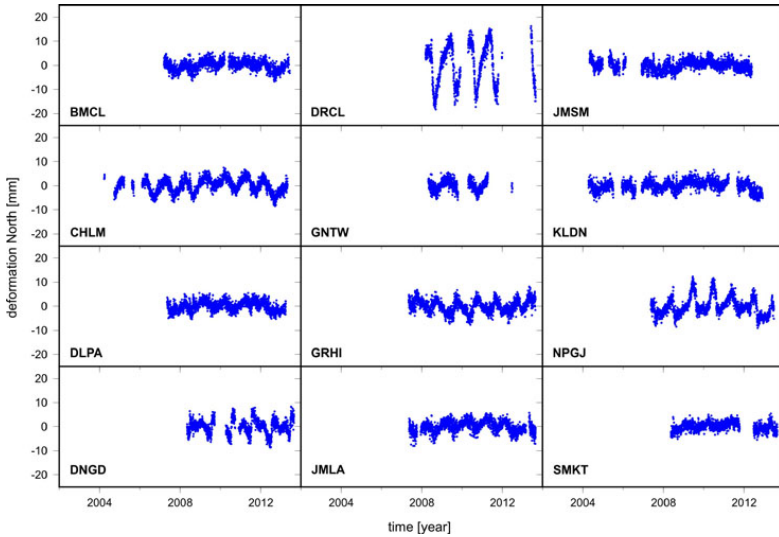


Fig. 2. North component of detrended time series of GNSS stations position

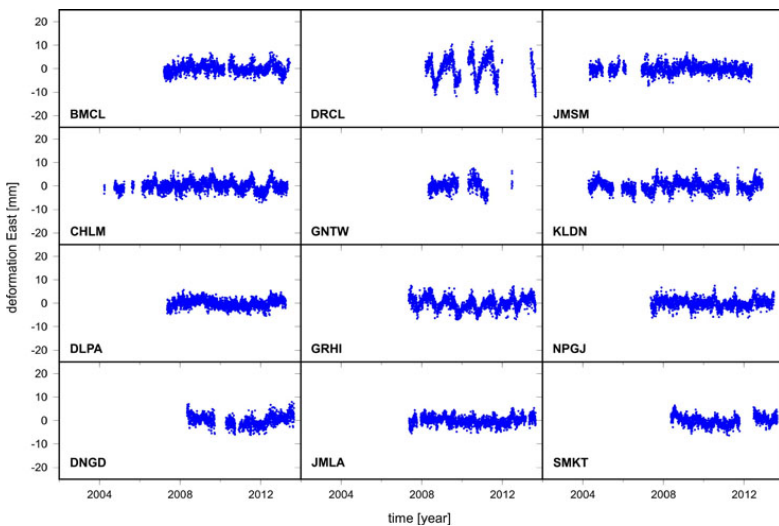


Fig. 3. East component of detrended time series of GNSS stations position

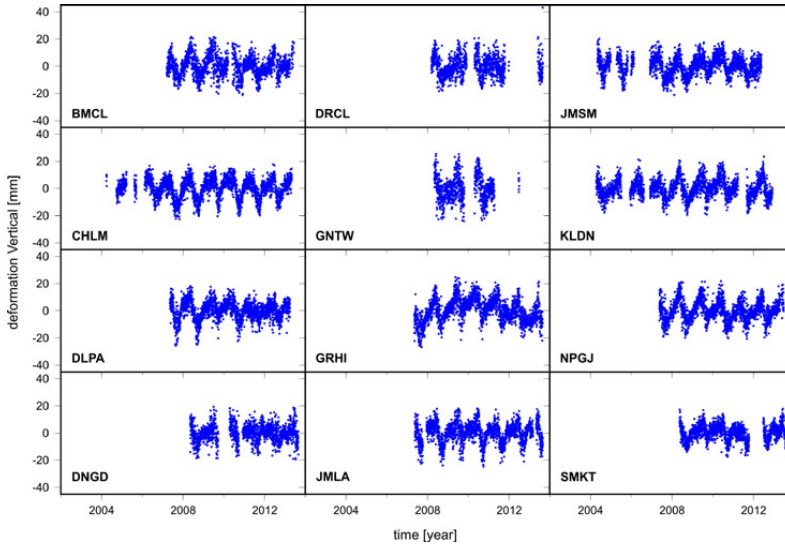


Fig. 4. Vertical component of detrended time series of GNSS stations position

3. Spectral analysis

There are two ways to obtain the power spectrum of a time series, depending on whether the data are evenly spaced or not (Mao et al., 1999). For evenly spaced data, the method used is given by discrete Fourier transform as (Scargle, 1982)

$$P(f_n) = \frac{1}{N} \left[\left(\sum_{j=1}^N x_j \cos 2\pi j f_n \right)^2 + \left(\sum_{j=1}^N x_j \sin 2\pi j f_n \right)^2 \right] \quad (2)$$

where $f_n = n/T$, T is the fundamental period, $n = 1, 2, 3, \dots, N/2$ and N is the number of observations.

In reality, the GNSS position time series (Figures 2–4) have, usually, data gaps due to various issues such as power failure, instrumental errors, etc. There are some obvious ways to make those unevenly spaced data to evenly ones. Interpolation is one way, but it fails in the case of large data gaps (Press et al., 1992). Within the course of this study, a method developed by Lomb (1976) and later elaborated by Scargle (1982) was employed. For a time series of N data points $x_j = x(t_j)$, observed at times t_j ; $j = 1, 2, \dots, N$, having mean \bar{x} , the Lomb–Scargle periodogram is given by (Mao et al., 1999)

$$P(f) = \frac{1}{2\sigma^2} \left[\frac{\left(\sum_j (x_j - \bar{x}) \cos 2\pi(t_j - \tau)f \right)^2}{\sum_j \cos^2 2\pi(t_j - \tau)f} + \frac{\left(\sum_j (x_j - \bar{x}) \sin 2\pi(t_j - \tau)f \right)^2}{\sum_j \sin^2 2\pi(t_j - \tau)f} \right] \quad (3)$$

where τ is defined by the relation

$$\tan(4\pi f\tau) = \frac{\sum_{j=1}^N \sin 4\pi t_j f}{\sum_{j=1}^N \cos 4\pi t_j f} \quad (4)$$

Scargle (1982) found that the resulting periodogram has exactly the same exponential probability distribution as the one of evenly spaced data. In earlier studies, such as Zhang et al. (1997) and Mao et al. (1999), spectral analysis was adopted to estimate spectral indices and thereby predicting the background noise model. Zhang et al. (1997) obtained the spectral index using a linear least square fit to the spectrum. The fit was, however, not able to capture the lower frequency part of the spectrum. In order to overcome the problem of linear least square, Mao et al. (1999) used iterative nonlinear least square fitting based on the Levenberg–Marquardt (LM) algorithm (Press et al., 1992) to estimate the spectral indices. Along with the spectral index, computed Hurst exponent is another frequently used characteristic to investigate the GNSS time series. The Hurst exponent introduced by Hurst (Hurst, 1951) and later used in fractal analysis (Mandelbrot and Wallis, 1969; Mandelbrot, 1983; Stan et al., 2014) is a numerical estimate to find the probability of time series (Akilan et al., 2013). The current investigation is, however, limited to the estimation of the spectral index. The iterative nonlinear LM algorithm (Press et al., 1992; Mao et al., 1999) was used to estimate the spectral index. The power spectra of the GNSS position time series used in the analysis along with the spectral indices of respective sites are illustrated in Figures 5–7. It is observed that power of the spectrum is inversely proportional to the frequency and represented well by power law. This may indicate that the spectrum of the GNSS position time series investigated can be described as white noise at high frequency and time correlated noise at low frequency. On an average, the power law noise extends up to a period of ca. 21 days and the spectra are white for a period shorter than ca. 21 days. The values of the spectral indices are given in Table 2. Mean and standard deviation of the spectral indices of all sites (excluding the DRCL) are -1.46 ± 0.14 , -1.39 ± 0.16 , and -1.53 ± 0.07 for the north, east, and vertical component, respectively. These spectral indices represent naturally occurring non stationary processes (Williams et al., 2004).

High values of spectral indices in horizontal components of DRCL (Figures 5, 6 and Table 2) indicate strong time-correlated processes with the nature of random walk, probably caused by a combination of tectonic (e.g. aseismic slips) and non-tectonic process ranging from the hydrological mass loading to monumental noise. It should be noted that monuments of all GNSS stations used in the current study are shallow drilled braced. Thus, for the DRCL station the higher value of spectral index might be induced by an external source in addition to the monumental motion. Although Williams et al. (2004) found that deep drill braced monuments are having high stability with less random walk amplitude compared to other types of monuments, it will be premature to attribute the

Table 2. Values of spectral indices estimated for North, East, and Vertical component of GNSS time series

Site	North	East	Vertical
BMCL	-1.39 ± 0.55	-1.47 ± 0.72	-1.50 ± 0.58
CHLM	-1.31 ± 0.76	-1.29 ± 0.53	-1.79 ± 0.61
DLPA	-1.29 ± 0.97	-1.21 ± 0.99	-1.11 ± 0.82
DNGD	-1.56 ± 0.48	-1.50 ± 0.99	-1.49 ± 0.46
DRCL	-2.15 ± 0.72	-2.02 ± 0.82	-1.19 ± 0.66
GNTW	-1.56 ± 0.70	-1.37 ± 0.72	-1.22 ± 0.68
GRHI	-1.83 ± 0.69	-1.81 ± 0.68	-1.26 ± 0.82
JMLA	-1.69 ± 0.69	-1.70 ± 0.62	-1.31 ± 0.59
JMSM	-1.30 ± 0.62	-1.29 ± 0.59	-1.67 ± 0.60
KLDN	-1.30 ± 0.89	-1.32 ± 0.53	-1.33 ± 0.51
NPGJ	-1.55 ± 0.88	-1.32 ± 0.57	-1.35 ± 0.52
SMKT	-1.49 ± 0.80	-1.46 ± 0.59	-1.24 ± 0.58

high spectral index values of the DRCL to the pure monumental noise as prediction or detection of random walk noise due to monumental motion requires longer time series (Langbein, 2012). However, Panda et al. (2018) observed abnormal seasonal transients in the horizontal component of the DRCL and suggest a change in a seismic slip rate controlled by hydrological loading. The high value of spectral index at the DRCL which is located above the base of a seismogenic zone can be due to the change of aseismic slip rate induced by the seasonal hydrological mass loading.

From the spectral analysis, the overall noise model for the GNSS position time series of permanent GNSS stations in Nepal Himalayan can be expressed as white noise plus power law noise. It should be mentioned that power law noise in many studies comes out to be flicker noise with no or very little random walk noise (Zhang et al., 1997; Williams et al., 2004; Amiri-Simkooei et al., 2007; Hackl et al., 2011). Thus, power law noise obtained within the course of this analysis seems to be a combination of flicker noise and random walk noise. The underlying physical process responsible for time correlated noise in the GNSS position time series could be ascribed to the seasonal hydrological mass change caused by monsoon precipitation.

Overall, results presented in Figures 5–7 reveal that the method of spectral analysis provides a possible noise model that can describe the GNSS position time series, which can then be used as *a priori* information while estimating realistic velocity uncertainties using the GAMIT/GLOBK software. The time correlated noise is accommodated in the GAMIT/GLOBK software through incorporation of a random walk noise to the error model used by the GLOBK software.

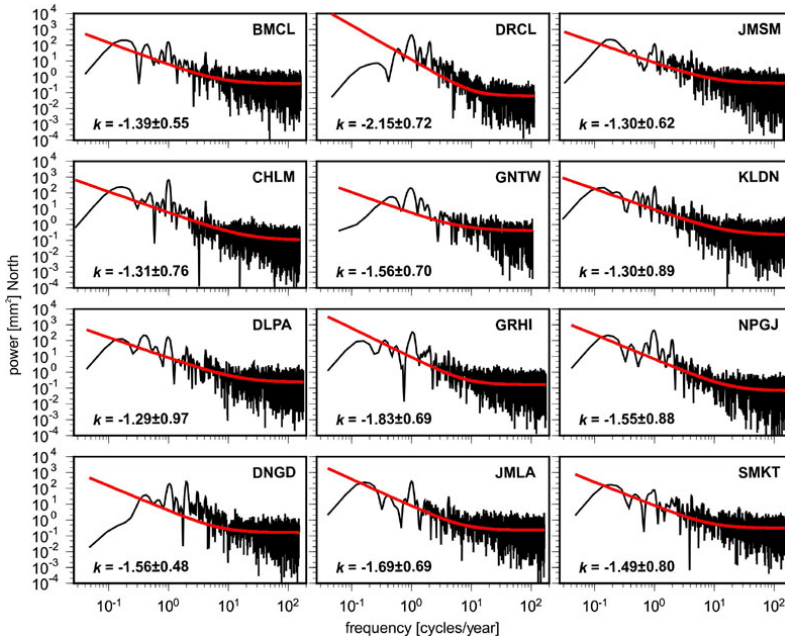


Fig. 5. Power spectrum of the GNSS position time series in the north component. Black curve is the power spectra and red curve is the Levenberg–Marquardt fit to the spectrum, k is the estimated spectral index

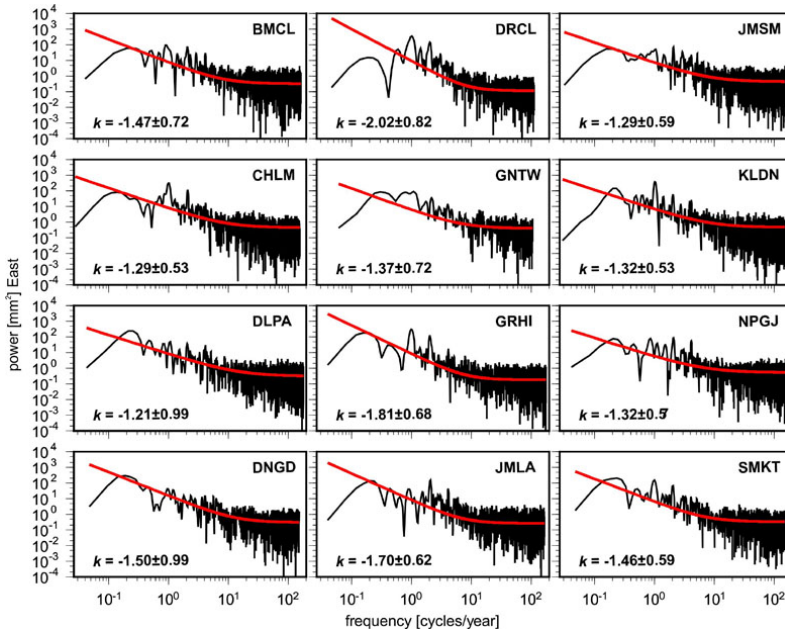


Fig. 6. Power spectrum of the GNSS position time series in the east component. Black curve is the power spectra and red curve is the Levenberg–Marquardt fit to the spectrum, k is the estimated spectral index

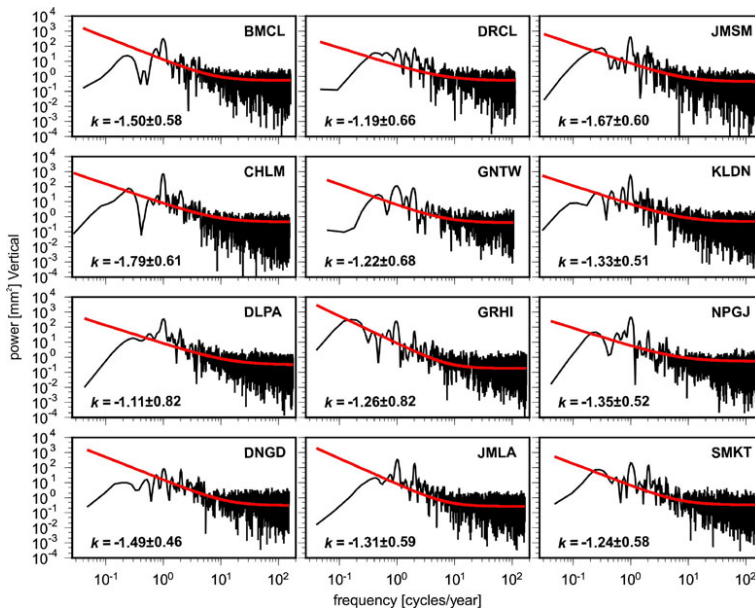


Fig. 7. Power spectrum of the GNSS position time series in the vertical component. Black curve is the power spectra and red curve is the Levenberg–Marquardt fit to the spectrum, k is the estimated spectral index

4. Conclusions

GNSS position time series from thirteen permanent GNSS stations in Nepal Himalaya were analyzed to study the background noise using spectral analysis. The power spectrum of the GNSS position time series obtained using the Lomb–Scargle periodogram can be described as white in high frequency zone and coloured in the low frequency regime. On an average, the power law noise extends up to a period of ca. 21 days and for periods shorter than 21 days spectra are white. Spectral analysis of the position time series suggests white plus power law process with mean and standard deviation of the spectral index of -1.46 ± 0.14 in the north component, -1.39 ± 0.16 in the east component and -1.53 ± 0.07 in the vertical component. High value of spectral index in the horizontal component of the DRCL can be attributed to the combined effect of an ongoing tectonic and non-tectonic process which needs a detailed investigation. The combination of the tectonic and non-tectonic process may cause change in a seismic slip rate which can give rise to the highest value of spectral index at the DRCL. The special case of the DRCL is an example of true physical cause of random walk noise rather than spurious monumental motion. The monuments of GNSS stations located in Nepal Himalayan are all shallow drilled braced and warrant a detail investigation of monumental behaviour with longer span of data is needed. Overall, the spectral analysis provides essential information about the background noise in GNSS position time series which can be used as *a priori* information while estimating realistic velocity uncertainties using the GAMIT/GLOBK software.

Acknowledgments

The authors are profoundly thankful to the University NAVSTAR Consortium (UNAVCO) for making the data publicly available with easily accessible interface to the data archive. We thank Jean Philippe Avouac and his group at Caltech Tectonics Observatory for establishing, and maintaining the GNSS stations in Nepal and opening up the data for public use. The first and third authors are financially supported by the Polish National Science Centre (NCN) within the research Grant No. 2017/26/D/ST10/00422. The authors are thankful to Prof. Jan Krynski from the IGIK for his valuable and helpful advices concerning this research.

References

- Ader, T., Avouac, J-P., Liu-Zeng, J., Lyon-Caen, H., Bollinger, L., Galetzka, J., Genrich, J., Thomas, M., Chanard, K., Sapkota, S.N., Rajaure, S., Shrestha, P., Ding, L. and Flouzat M. (2012). Convergence rate across the Nepal Himalaya and interseismic coupling on the Main Himalayan Thrust: Implications for seismic hazard. *Journal of Geophysical Research: Solid Earth*, 117, B04403. DOI: [10.1029/2011JB009071](https://doi.org/10.1029/2011JB009071).
- Agnew, D.C. (1992). The time-domain behavior of power-law noises. *Geophysical Research Letters*, 19 (4), 333–336. DOI: [10.1029/91GL02832](https://doi.org/10.1029/91GL02832).
- Akilan, A., Balaji, S., Srinivas, Y. and Yuvaraj, N. (2013). Plate motion predictability using Hurst exponent applied to the Maitri-antarctica GPS network. *Journal of the Geological Society of India*, 82 (6), 613–620. DOI: [10.1007/s12594-013-0199-z](https://doi.org/10.1007/s12594-013-0199-z).
- Altamimi, Z., Collilieux, X. and Métivier, L. (2011). ITRF2008: an improved solution of the international terrestrial reference frame. *Journal of Geodesy*, 85 (8), 457–473. DOI: [10.1007/s00190-011-0444-4](https://doi.org/10.1007/s00190-011-0444-4).
- Amiri-Simkooei, A.R., Tiberius, C.C.J.M. and Teunissen, S.P. (2007). Assessment of noise in GPS coordinate time series: methodology and results. *Journal of Geophysical Research: Solid Earth*, 112(B7), B07413. DOI: [10.1029/2006JB004913](https://doi.org/10.1029/2006JB004913).
- Avouac, J-P., Adhikari, L.B., Galetzka, J.E., Koirala, B., Shrestha, P., Gupta, R.M., Gautam, U., Flouzat, M., Bollinger, L., Bhattarai, M., Kandel, T., Timsina, C., Sapkota, S.N., Rajaure, S., Genrich, J.F. and Maharjan, N. (2013). Caltech Tectonics Observatory Nepal Network – NEGAR – SYBC-Syangboche P.S., UNAVCO, Inc., GPS/GNSS Observations Dataset. DOI: [10.7283/T5222RX3](https://doi.org/10.7283/T5222RX3).
- Beavan, J. (2005). Noise properties of continuous GPS data from concrete pillar geodetic monuments in New Zealand and comparison with data from U.S. deep drilled braced monuments. *Journal of Geophysical Research*, 110, 08410. DOI: [10.1029/2005JB003642](https://doi.org/10.1029/2005JB003642).
- Bettinelli, P., Avouac, J-P., Flouzat, M., Jouanne, F., Bollinger, L. and Willis, P. (2006). Plate Motion of India and Interseismic Strain in the Nepal Himalaya from GPS and DORIS Measurements. *Journal of Geodesy*, 80(8–11), 567–589. DOI: [10.1007/s00190-006-0030-3](https://doi.org/10.1007/s00190-006-0030-3).
- Bogusz, J., Rosat, S., Klos, A. and Lenczuk, A. (2018). On the noise characteristics of time series recorded with nearby located GPS receivers and superconducting gravity meters. *Acta Geodaetica et Geophysica*, 53(2), 201–220. DOI: [10.1007/s40328-018-0212-5](https://doi.org/10.1007/s40328-018-0212-5).
- Böhm, J., Heinkelmann, R. and Schuh, H. (2007). Short Note: A global model of pressure and temperature for geodetic applications. *Journal of Geodesy*, 81(10), 679–683. DOI: [10.1007/s00190-007-0135-3](https://doi.org/10.1007/s00190-007-0135-3).
- Dmitrieva, K., Segall, P. and DeMets, C.J. (2015). Network-based estimation of time-dependent noise in GPS position time series. *Journal of Geodesy*, 89(6), 591–606. DOI: [10.1007/s00190-015-0801-9](https://doi.org/10.1007/s00190-015-0801-9).

- Finlay, C.C., Maus, S., Beggan, C.D., Bondar, T.N., Chambodut, A., Chernova, T.A., Chulliat, A., Golovkov, V.P., Hamilton, B., Hamoudi, M., Holme, R., Hulot, G., Kuang, W., Langlais, B., Lesur, V., Lowes, F.J., Lühr, H., Macmillan, S., Manda, M., McLean, S., Manoj, C., Menvielle, I., Michaelis, N., Olsen, J., Rauberg, M., Rother, T., Sabaka, J., Tangborn, A., Tøffner-Clausen, L.M., Thébaud, E., Thomson, A.W.P., Wardinski, I., Wei, Z. and Zvereva, T.I., (2010). International Geomagnetic Reference Field: the eleventh generation. *Geophysical Journal International*, 183(3), 1216–1230. DOI: [10.1111/j.1365-246X.2010.04804.x](https://doi.org/10.1111/j.1365-246X.2010.04804.x).
- Fritsche, M., Dietrich, R., Knöfel, C., Rülke, A., Vey, S., Rothacher, M. and Steigenberger, P. (2005). Impact of higher-order ionospheric terms on GPS estimates. *Geophysical Research Letters*, 32(23), L23311. DOI: [10.1029/2005GL024342](https://doi.org/10.1029/2005GL024342).
- Hackl, M., Malservisi, R., Hugentobler, U. and Wonnacott, R. (2011). Estimation of velocity uncertainties from GPS time series: Examples from the analysis of the South African TrigNet network. *Journal of Geophysical Research: Solid Earth*, 116 (B11), B11404. DOI: [10.1029/2010JB008142](https://doi.org/10.1029/2010JB008142).
- Herring, T.A., King, R.W. and McClusky, S.C. (2010). Introduction to GAMIT/GLOBK release 10.4. Department of Earth, and Planetary Sciences, MIT, Cambridge, USA. https://geo.gob.bo/portal/IMG/pdf/intro_gg_1_.pdf.
- Hurst, H.E. (1951). Long-term storage capacity of reservoirs. *Transactions of the American Society of Civil Engineers*, 116(1), 770–799.
- Jiang, W., Deng, L., Li, Z., Zhou, X. and Liu, H. (2014). Effects on noise properties of GPS time series caused by higher-order ionospheric corrections. *Advances in Space Research*, 53 (7), 1035–1046. DOI: [10.1016/j.asr.2013.12.037](https://doi.org/10.1016/j.asr.2013.12.037).
- Johnson, H.O. and Agnew, D.C. (1995). Monument motion and measurements of crustal velocities. *Geophysical Research Letters*, 22(21), 2905–2908. DOI: [10.1029/95GL02661](https://doi.org/10.1029/95GL02661).
- King, M.A. and Williams, S. (2009). Apparent stability of GPS monumentation from short-baseline time series. *Journal of Geophysical Research: Solid Earth*, 114(B10), 10403. DOI: [10.1029/2009JB006319](https://doi.org/10.1029/2009JB006319).
- Klos, A., Bogusz, J., Figurski, M. and Kosek, W. (2015). Irregular variations in GPS time series by probability and noise analysis. *Survey Review*, 47(342), 163–173. DOI: [10.1179/1752270614Y.0000000133](https://doi.org/10.1179/1752270614Y.0000000133).
- Kouba, J. (2008). Implementation and testing of the gridded Vienna mapping function 1 (VMF1). *Journal of Geodesy*, 82 (4–5), 193–205. DOI: [10.1007/s00190-007-0170-0](https://doi.org/10.1007/s00190-007-0170-0).
- Langbein, J. and Johnson, H. (1997). Correlated errors in geodetic time series: Implications for time-dependent deformation. *Journal of Geophysical Research: Solid Earth*, 102 (B1), 591–603. DOI: [10.1029/96JB02945](https://doi.org/10.1029/96JB02945).
- Langbein, J. (2012). Estimating rate uncertainty with maximum likelihood: differences between power-law and flicker-random-walk models. *Journal of Geodesy*, 86(9), 775–783. DOI: [10.1007/s00190-012-0556-5](https://doi.org/10.1007/s00190-012-0556-5).
- Lomb, N.R. (1976). Least-squares frequency analysis of unequally spaced data. *Astrophysics and Space Science*, 39 (2), 447–462. DOI: [10.1007/BF00648343](https://doi.org/10.1007/BF00648343).
- Mandelbrot, B.B. (1983). *The fractal geometry of nature*. New York: WH Freeman and Company.
- Mandelbrot, B.B. and van Ness, J.W. (1968). Fractional Brownian motions, fractional noises and applications. *SIAM review*, 10 (4), 422–437. DOI: [10.1137/1010093](https://doi.org/10.1137/1010093).
- Mandelbrot, B.B. and Wallis, J.R. (1969). Some Long-Run Properties Geophysical Record. *Water Resources Research*, 5 (5), 321–340. DOI: [10.1029/WR005i002p00321](https://doi.org/10.1029/WR005i002p00321).
- Mao, A., Harrison, C.G. and Dixon, T.H. (1999). Noise in GPS coordinate time series. *Journal of Geophysical Research: Solid Earth*, 104 (B2), 2797–2816. DOI: [10.1029/2009JB006319](https://doi.org/10.1029/2009JB006319).
- Panda, D., Kundu, B., Gahalaut, V.K., Bürgmann, R., Jha, B., Asaithambi, R. and Bansal, A.K. (2018). Seasonal modulation of deep slow-slip and earthquakes on the Main Himalayan Thrust. *Nature communications*, 9(9), 4140.

- Press, W.H., Teukolsky, S.A., Vetterling, W.T. and Flannery, B.P. (1992). Numerical recipes: The art of scientific computing (3rd ed.). Cambridge, United Kingdom: Cambridge University press.
- Ray, J., Altamimi, Z., Collilieux, X. and van Dam, T. (2008). Anomalous harmonics in the spectra of GPS position estimates. *GPS Solutions*, 12(1), 55–64. DOI: [10.1007/s10291-007-0067-7](https://doi.org/10.1007/s10291-007-0067-7).
- Ray, J., Vijayan, M.S.M. and Kumar, A. (2019). Noise characteristics of GPS time series and their influence on velocity uncertainties. *Journal of Earth System Science*, 128, 146. DOI: [10.1007/s12040-019-1179-5](https://doi.org/10.1007/s12040-019-1179-5).
- Rebischung, P., Chanard, K., Metivier, L. and Altamimi, Z. (2017). Flicker Noise in GNSS Station Position Time Series: How much is due to Crustal Loading Deformations? American Geophysical Union, New Orleans, USA, 11–15 December 2017, abstract No G13A-04.
- Saastamoinen, J., (1972). Atmospheric correction for the troposphere and stratosphere in radio ranging satellites. [In:] Henriksen S.W., Mancini A., Chovitz B.H. (eds.), *The use of artificial satellites for geodesy*, Geophysical Monograph Series, 15, 247–251. DOI: [10.1029/GM015p0247](https://doi.org/10.1029/GM015p0247).
- Santamaría-Gómez, A., Bouin, M.N., Collilieux, X. and Wöppelmann, G. (2011). Correlated errors in GPS position time series: implications for velocity estimates. *Journal of Geophysical Research: Solid Earth*, 116 (B1), B01405. DOI: [10.1029/2010JB007701](https://doi.org/10.1029/2010JB007701).
- Scargle, J.D. (1982). Studies in astronomical time series analysis. II-Statistical aspects of spectral analysis of unevenly spaced data. *Astrophysical Journal*, 263, 835–853.
- Schaer, S., Gurtner, W. and Feltens, J. (1998). IONEX: The IONosphere Map EXchange Format Version 1. Proc. of the IGS AC Workshop, Darmstadt, Germany, 9–11 February 1998. <http://ftp.aiub.unibe.ch/ionex/ionex1.pdf>.
- Stan, C., Cristescu, C-M. and Cristescu, C. (2014). Computation of hurst exponent of time series using delayed (log-) returns. Application to estimating the financial volatility. *University Politechnica of Bucharest Scientific Bulletin*, 76(3), 235–244.
- Wang, W., Zhao, B., Wang, Q. and Yang, S. (2012). Noise analysis of continuous GPS coordinate time series for CMONOC. *Advances in Space Research*, 49 (5), 943–956. DOI: [10.1016/j.asr.2011.11.032](https://doi.org/10.1016/j.asr.2011.11.032).
- Williams, S.D. (2003). Offsets in global positioning system time series. *Journal of Geophysical Research: Solid Earth*, 108 (B6), 2310. DOI: [10.1029/2002JB002156](https://doi.org/10.1029/2002JB002156).
- Williams, S.D., Bock, Y., Fang, P., Jamason, P., Nikolaidis, R.M., Prawirodirdjo, L., Miller, M. and Johnson, D.J., (2004). Error analysis of continuous GPS position time series. *Journal of Geophysical Research: Solid Earth*, 109 (B3), B03412. DOI: [10.1029/2003JB002741](https://doi.org/10.1029/2003JB002741).
- Zhang, J., Bock, Y., Johnson, H., Fang, P., Williams, S., Genrich, J., Wdowinski, S. and Behr, J., (1997). Southern California Permanent GPS Geodetic Array Error analysis of daily position estimates and site velocities. *Journal of Geophysical Research: Solid Earth*, 102 (B8), 18035–18055. DOI: [10.1029/97JB01380](https://doi.org/10.1029/97JB01380).